International Association of Geodesy Symposia

Fernando Sansò, Series Editor

International Association of Geodesy Symposia

Fernando Sansò, Series Editor

Symposium 101: Global and Regional Geodynamics
Symposium 102: Global Positioning System: An Overview
Symposium 103: Gravity, Gradiometry, and Gravimetry
Symposium 104: Sea SurfaceTopography and the Geoid
Symposium 105: Earth Rotation and Coordinate Reference Frames
Symposium 106: Determination of the Geoid: Present and Future
Symposium 107: Kinematic Systems in Geodesy, Surveying, and Remote Sensing
Symposium 108: Application of Geodesy to Engineering
Symposium 109: Permanent Satellite Tracking Networks for Geodesy and Geodynamics
Symposium 110: From Mars to Greenland: Charting Gravity with Space and Airborne Instruments
Symposium 111: Recent Geodetic and Gravimetric Research in Latin America
Symposium 112: Geodesy and Physics of the Earth: Geodetic Contributions to Geodynamics
Symposium 113: Gravity and Geoid
Symposium 114: Geodetic Theory Today
Symposium 115: GPS Trends in Precise Terrestrial, Airborne, and Spaceborne Applications
Symposium 116: Global Gravity Field and Ist Temporal Variations
Symposium 117: Gravity, Geoid and Marine Geodesy
Symposium 118: Advances in Positioning and Reference Frames
Symposium 119: Geodesy on the Move
Symposium 120: Towards an Integrated Global Geodetic Observation System (IGGOS)
Symposium 121: Geodesy Beyond 2000: The Challenges of the First Decade
Symposium 122: IV Hotine-Marussi Symposium on Mathematical Geodesy
Symposium 123: Gravity, Geoid and Geodynamics 2000
Symposium 124: Vertical Reference Systems
Symposium 125: Vistas for Geodesy in the New Millennium
Symposium 126: Satellite Altimetry for Geodesy, Geophysics and Oceanography
Symposium 127: V Hotine Marussi Symposium on Mathematical Geodesy
Symposium 128: A Window on the Future of Geodesy
Symposium 129: Gravity, Geoid and Space Missions

Gravity, Geoid and Space Missions

GGSM 2004
IAG International Symposium
Porto, Portugal
August 30 - September 3, 2004

Edited by
Christopher Jekeli
Luisa Bastos
Joana Fernandes

Springer

Volume Editors

Professor Christopher Jekeli
Geodetic Science
Ohio State University
470 Hitchcock Hall
2070 Neil Ave.
Columbus, OH 43210
USA

Dr. Luisa Bastos
Faculdade de Ciências da Universidade Porto
Observatório Astronómico
Alameda do Monte da Virgem
4430-146 V.N. GAIA
Portugal

Professor Joana Fernandes
Faculdade de Ciências da Universidade Porto
Departamento de Matemática Aplicada
Rua do Campo Alegre 687
4169-007 Porto
Portugal

Series Editor

Professor Fernando Sansò
Polytechnic of Milan
D.I.I.A.R. – Surveying Section
Piazza Leonardo da Vinci, 32
20133 Milan
Italy

Library of Congress Control Number: 2005927793

ISSN 0939-9585
ISBN 3-540-26930-4 Springer Berlin Heidelberg New York

Springer is a part of Springer Science+Business Media
springeronline.com

Printed in Germany

Cover design: design & production GmbH, Heidelberg
Production: Almas Schimmel
Typesetting: Camera ready by the authors
Printing and Binding: Mercedes-Druck, Berlin

Printed on acid-free paper 32/3141/as 5 4 3 2 1 0

Preface

The IAG International Symposium on Gravity, Geoid, and Space Missions 2004 (GGSM2004) was held in the beautiful city of Porto, Portugal, from 30 August to 3 September 2004. This symposium encompassed the themes of Commission 2 (Gravity Field) of the newly structured IAG, as well as interdisciplinary topics related to geoid and gravity modeling, with special attention given to the current and planned gravity-dedicated satellite missions. The symposium also followed in the tradition of mid-term meetings that were held between the quadrennial joint meetings of the International Geoid and Gravity Commissions. The previous mid-term meetings were the International Symposia on Gravity, Geoid, and Marine Geodesy (Tokyo, 1996), and Gravity, Geoid, and Geodynamics (Banff, 2000).

GGSM2004 aimed to bring together scientists from different areas in the geosciences, working with gravity and geoid related problems, both from the theoretical and practical points of view. Topics of interest included the integration of heterogeneous data and contributions from satellite and airborne techniques to the study of the spatial and temporal variations of the gravity field. In addition to the special focus on the CHAMP, GRACE, and GOCE satellite missions, attention was also directed toward projects addressing topographic and ice field mapping using SAR, LIDAR, and laser altimetry, as well as missions and studies related to planetary geodesy.

The Science Committee for the Symposium comprised Christopher Jekeli (President), Ilias N. Tziavos, Roger Haagmans, René Forsberg, Luisa Bastos, and Joana Fernandes, while its local organization was under the direction of Luisa Bastos, Joana Fernandes and Machiel Bos of the Faculty of Science, University of Porto. In addition, many colleagues associated with Commission 2 and the IAG organized the nine sessions of the Symposium as follows:

1. Gravity field modeling from satellite missions
   Pieter Visser (Delft University of Technology, The Netherlands)
   Roger Haagmans (ESA, The Netherlands)

2. Airborne and satellite gravimetry instrumentation
   René Forsberg (Geodynamics Department, Danish National Space Center)
   Luisa Bastos (University of Porto, Portugal)

3. Regional geoid modeling
   Urs Marti (Swiss Federal Office of Topography, Switzerland)
   Ilias Tziavos (Aristotle University of Thessaloniki, Greece)

4. Radar and laser surface mapping from satellites
   Philippa Berry (De Montfort University, U.K.)
   Bill Carter (University of Florida, U.S.A.)

5. Topographic data bases and gravity modeling
   Steve Kenyon (NGA, U.S.A.)
   Per Knudsen (KMS, Denmark)

6. Satellite altimetry, oceanography, and the geoid
   Dave Sandwell (University of California, San Diego, U.S.)
   Joana Fernandes (University of Porto, Portugal)

7. Terrestrial gravity instrumentation, networks, and geodynamics
   Shuhei Okubo (Earthquake Research Institute, University of Tokyo, Japan)
   Tonie van Dam (European Centre for Geodynamics and Seismology, Luxemburg)

8. Temporal gravity variations: modeling and measurements
   C.K. Shum (Ohio State University, U.S.A.)
   Martin Vermeer (Helsinki University of Technology, Switzerland)

9. Planetary gravity fields and models
   Dave Smith (NASA, U.S.A.)
   Georges Balmino (CNES, France)

The Symposium attracted 258 papers, of which 108 were presented orally and 150 as posters. It was truly an international scientific event as all six continents and 39 countries were represented by a total of 234 participants. A Proceedings of the Symposium was published in the form of a CD with most of the oral and poster presentations, as well as many corresponding journal-style papers. Of the latter, a portion were selected and reviewed for inclusion in this volume and they represent the high level of activity and advanced research in gravity and geoid modeling that was displayed by all contributions to this symposium. Although Session 9 papers were not submitted to this volume it is anticipated that the relationship between gravity field modeling and planetary geodesy particularly encouraged in this symposium will be strengthened in future symposia and other similar events.

Special recognition and gratitude go to the Session co-conveners whose hard work in organizing their sessions and guiding the reviews of the submitted papers resulted in a very successful Symposium and a high quality scientific volume. The organization of a Symposium of this magnitude is never easy, but it unfolded flawlessly due to the expert preparation and continual attentiveness of the organizing committee, headed by Luisa Bastos, Joana Fernandes and Machiel Bos. The collection of material for the CD Proceedings and the assembly of the papers for this volume was also done professionally and efficiently and special thanks are due the Faculty of Science, University of Porto, for helping to support these publications.

The success of the Symposium also depends to a great extent on the financial sponsorship of interested and supporting organizations and institutions in the form of cash and travel re-imbursements, especially for students and colleagues from developing countries. We

gratefully acknowledge financial contributions from IAG, IUGG, NASA, ESA, GRICES, FCT and the University of Porto.

Finally, I wish to extend my personal appreciation and congratulations to Luisa Bastos, Joana Fernandes and Machiel Bos for their devotion to this symposium and their perseverance in completing the publications. It is not easy, even in these modern times, to coordinate such affairs over intercontinental distances, but they maintained a schedule and succeeded splendidly in every respect.

Christopher Jekeli Ohio State University, March 2005

Contents

Session 1:

Initial results from retracking and reprocessing the ERS-1 geodetic mission altimetry for gravity field purposes.

Ole B. Andersen, P. Knudsen,
Danish Space Center, Juliane Mariesvej 30, DK-2100 Copenhagen, Denmark. Email: oa@spacecenter.dk,

P. A. M. Berry, E. L. Mathers. EAPRS Laboratory, De Montfort University, The Gateway, Leicester. LE1 9BH, UK.

R. Trimmer, S. Kenyon
National Geospatial-Intelligence Agency, GIMG, St Louis. MS, USA

Abstract. All present global marine gravity fields are based on the 1Hz ERS-1 Geodetic Mission (GM) altimeter data combined with other altimetric datasets. Close to the coast (<25 km) this investigation shows that the altimetric gravity field determination degrades due to a combination of several factors, where the main reason is the degradation of the quality of the altimeter data. By starting out from the original waveform data and retracking the entire ERS-1 GM mission using a highly advanced expert based system of multiple retrackers, the return time from both open ocean and coastal sea surface as well as from all ice-covered regions within the coverage of the ERS-1 can be derived with higher accuracy than presently available.
Initial results of the combined effort to improve the ERS-1 GM altimetric dataset through retracking and regression to 2Hz (3km) are presented, and its effort on gravity field modeling close to the coast and in Polar Regions is discussed. Close to the coast and in particular in Polar Regions the use of multiple retrackers leads to considerably more and better data than in the normal 1 Hz data delivered by the European Space Agency (ESA).
Extensive comparison with marine gravity field data by the National Geospatial-Intelligence Agency is also presented to document the improvement on gravity field determination

Keywords. Satellite altimetry, retracking, gravity field determination, coastal, polar regions.

1 Introduction

One of the outstanding problems in global marine gravity field determination is the degradation of the gravity field close to the coast as well as in Polar Regions.

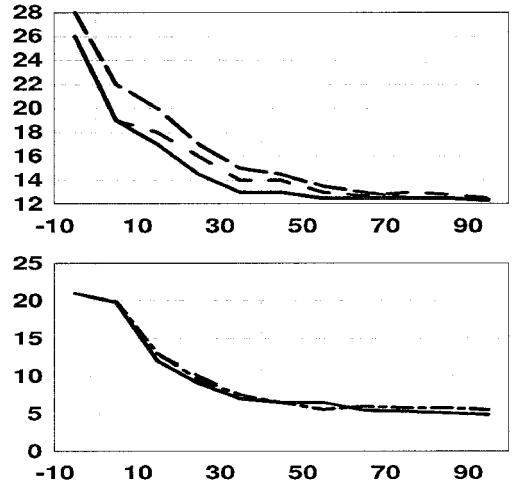

Figure 1. Standard deviation (mGal) of gravity comparison with marine data as a function of depth in meters (upper figure) and distance in kilometers to the coast (lower figure). The fields are KMS99 (Andersen and Knudsen, 1998) as solid line, SS 11.2 (Sandwell and Smith, 1997) long dash, and GSFC00.1 (Wang, 2000) short dash

Figure 1 shows the standard deviation of different global gravity fields as a function of depth (upper figure) and distance to the shore (lower figure) for coastal regions. The comparison with global marine gravity fields has been carried out with more than

1000 marine gravity observations in each 10 m depth or 10 km distance interval on the x-axis. In both figures the coast is to the left. For both the comparison with depth and distance, there is clear degradation in the accuracy from roughly 25 km to the coast in terms of distance, or for depths shallower than 20 meters. The degradation can be directly related to the degradation of the coverage and accuracy of the altimetric observations. Overall, the largest contributors are as follows:

1. Lack of data due to editing and automatic criteria applied to data.
2. Errors due to bad retracking of the data.
3. Change in sea state /ocean variability.
4. Errors in applied models for geophysical and range corrections, particularly the tidal model

Besides these altimetric related problems, there will be errors in the gravity field computation due to the presence of the coast, combined with the use of approximate methods which are required because the vast number of datapoints (mainly FFT methods).

The papers by Andersen et al., (1999, 2004) deal with the effect on gravity field modelling from improving the corrections applied to the altimetric observations.

In this paper we will present a way to improve the coverage of data in shallow water and Polar Regions, and the errors due to bad retracking. Several other scientific groups are currently investigating the use of retracking to enhance the quality of the altimetric observation from the ERS-1 geodetic mission altimetry. The current Sandwell and Smith (1997) global marine gravity field version 11.2 is produced from retracked ERS-1 altimetry. Laxon and McAdoo (1998) have retracked altimetry in the Arctic Ocean, Hwang (2003) has retracked altimetry in the China Sea, and Fairhead et al. (2004) have retracked data in several coastal regions.

Our methods differs from all the approaches above, as it includes a full retracking of the 20 Hz waveform data for the whole ERS-1 Geodetic Mission data (GM) using a suite of different retrackers for different conditions, with the use of a new method to regress these data onto 1 or 2 Hz values. We will show initial results to demonstrate the improvement in gravity field determination in a test region around Hawaii. Finally we will demonstrate the importance of retracking on data coverage in Polar Regions.

2 Retracking the ERS-1 GM data.

Whilst individual open ocean echoes generally correspond well to a mathematical model, which enables precise range to surface information to be retrieved, echoes in coastal zones are frequently distorted and therefore fail the standard automated processing procedures, and are rejected.

A variety of different echo shapes appear in the coastal zones caused by a variety of surface effects: these include land contamination of the echo, off-ranging to inland water, and the presence of unusually calm water in sheltered areas. However, although coastal zone echoes are complex and rapidly changing, almost all these waveforms can be successfully retracked. Within 5 km of the coastline, the majority of waveforms do not conform to the normal ocean model echo shape and are hence not retracked in the original data provided by ESA.

The EAPRS rule-based expert system (Berry et al., 1997) was designed to retrack the complex waveform shapes collected over land. Recently, the SOC ocean retracker (Challenor and Srokosz, 1989) has been added to the system, which now contains 11 retracking algorithms making the system capable of retracking waveforms everywhere.

For the implemented SOC ocean retracker, the 5-point Maximum Likelihood Estimate fit was changed to a 3-point least-squares fit because thermal noise was suppressed on ERS-1, and the bottom part of the leading edge is missing (so sea surface skewness cannot be calculated).

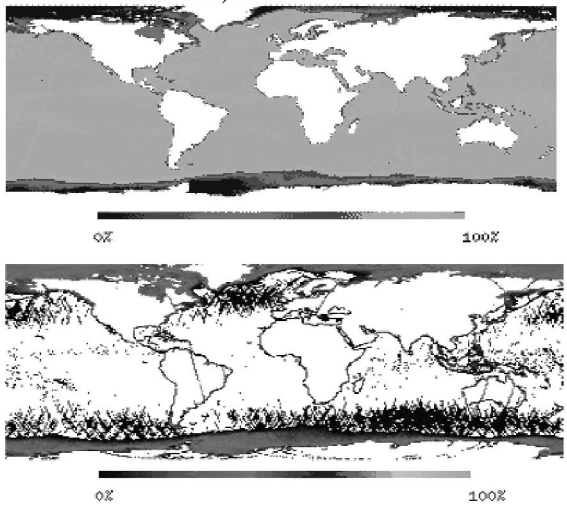

Figure 2 Percentage of the total number of points retracked using two different retrackers in the ESPRS system. The upper figure is the number of data retrieved by the SOC ocean retracker, and the lower figure is the sea-ice retracker. The data in the lower figure are normally rejected from the altimeter data delivered by ESA.

Figure 2 shows the additional amount of data retrieved by the EAPRS system compared with the normal ocean retracking performed by ESA. The upper figure shows the percentage of data retrieved by the normal ocean retracking which is very close to 100 percent in the open ocean, and the lower figure shows the additional data obtained from one of the 10 additional retrackers in the EAPRS system. In this case it is the sea-ice retracker. Note that the sea-ice retracker turns on in small numbers in coastal regions and in the presence of strong currents. This is because the echoes are similar in shape to one category of sea-ice echoes.

3 Regressing altimetry onto 2Hz

With both the GEOSAT and the ERS-1 GM, the average track spacing between the combined set of tracks is around 4 km at the Equator. The distance between the 1 Hz individual altimetric observations along the track is 7 km. In order to increase the spatial resolution along track we decided to investigate the possibility of regressing the data onto 2 Hz values, which would give a 3.5 km distance between the observations. The 2Hz data would be computed from 10 observations versus 20 observations for the 1Hz average.

Normally, the 1 Hz average values are computed in fixed 1-second bins by removing the two observations furthest away from the mean and then by averaging the remaining observations. We propose to use an alternative technique for the computation of 2 Hz data, which is a local regression smoothing called "Loess" (Cleveland, 1979) which stands for local weighted linear regression to smooth data. The regression approach has the advantage over averaging, that it is possible to interpolate data closer to the coast (it only requires one 20 Hz observation closer to the coast). It furthermore uses a robust weight function that is resistant to outliers.

Initially gross-errors and data over land are removed by comparing with the KMS04 Mean sea surface height. The Loess scheme works by computing tricubic weigh functions for each 20 Hz observation depending on the along-track distance to the position to be computed (Cleveland, 1988). Subsequently, a linear least squares regression is performed using a first-degree polynomial. The smoothed or regressed point is then given as the weighed regression at the point of interest. By comparing all the residuals to the regressed point and computing the median of the absolute deviations, outliers can be detected and removed, and the regression can be repeated iteratively until all outliers have been removed.

4 Gravity field test around Hawaii.

Hawaii was chosen as the test region for the retracking and regression analysis as this region has very good marine gravity observations, and extreme gravity field changes, varying by more than 700 mGal across the islands.

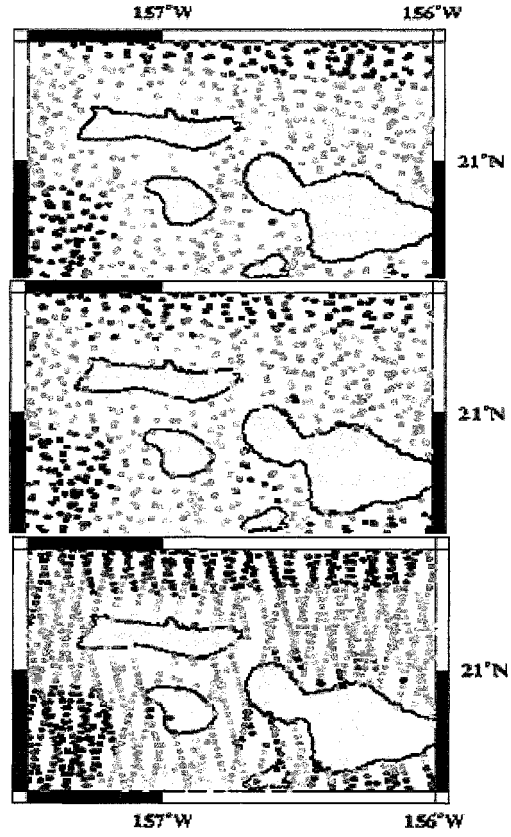

Figure 3 Residual geoid heights (to EGM96) of 1 Hz altimetric observations retracked by the ESA retracker (upper figure) and 1 Hz observations retracked by the EAPRS. (middle figure) and 2 Hz observations (lower figure).

Figure 3 shows crossover adjusted residual geoid height observations compared to EGM96 of the normal ESA retracked observations and the observations retracked by the EAPRS expert retracker system. The expert system clearly retracks more point close to the coast. There are however some visible differences, particularly at the on-set of new observations after passage of the islands. This is due to the fact that the ocean retrackers in the expert

system has not yet been adjusted properly, and hence shows an offset compared with the other retrackers. This is primarily expressed as a bias; the expert system is currently being tuned using a global ocean cross-calibration of retracker heights to remove this offset.

Table 1 Comparison with 76789 marine gravity observations within the Hawaii region. RADS indicate ESA retracked data. All values are in mGal.

	Mean	Std Dev	Max dev.
RADS	-1.76	12.82	144.53
EAPRS 1Hz	-2.11	12.59	156.21
EAPRS 2 Hz	-2.10	12.01	152.78

Table 1 shows a comparison with marine gravity observations within the Hawaii region bound by (15°<lat<29°, 188°<long<208°) in a gravity field computation following the methods by Andersen and Knudsen, (1998). Only ERS-1 GM data have been used for the gravity field computation.

Even with the known offset in one of the retrackers in the EAPRS system these data perform slightly better in a comparison with marine gravity observations that the ESA retracked data (12.82 to 12.59 mGal respectively).

With the additional enhancement of using 2 Hz data rather than 1 Hz data, further improvements are obtained (12.82 to 12.01 mGal respectively) which shows the importance of the increased data coverage in regions of large gravity field variations.

Further investigations in coastal regions is currently ongoing to substantiate and validitate these preliminary results as well as to fine-tune the dataediting and gravity predictions softward.

5 Polar Regions.

Retracking will provide the most new valuable observations in the Polar Regions where most observations fail to be retracked by the standard ESA ocean-model retracker when sea-ice is present. This was also demonstrated in Figure 2, which showed the number of additional data that could be retrieved with the sea-ice retracker.

Figure 4 shows the vast improvement in spatial coverage of good altimetric observations in complex coastal Polar Regions. The region east of Greenland is notorious for the presence of sea ice. It is roughly 600 km by 400 km in extent, and the number of ERS-1 data points that can be retrieved from retracking is increased from 350 datapoints to 11.200 datapoints when including, in particular, the sea-ice retracker. The figure also demonstrates apparent inaccuracies in the coastline model used for the plot, and illustrates the possibility of retracking data even in deep fjords, where altimetry has not previously been available.

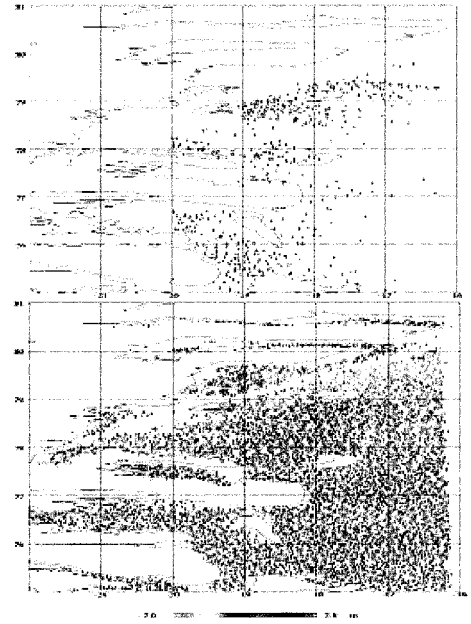

Figure 4 Unadjusted altimetric geoid height observations in the ice-covered regions east of Greenland. The upper figure shows the 1Hz data in the Radar Altimeter Database System (RADS), which uses the data delivered by the ESA retracking system, and the lower figure shows the 1 Hz retracked altimetric data.

A comparison with 1288 marine in the permanently ice-covered region east of Greenland is shown in Table 2. The Laxon and McAdoo (1998) polar gravity field and the KMS02 gravity field were included. In this region the great impact of retracking is clearly demonstrated. For KMS02 the lack of ocean retracked altimetry shows that this field is not an improvement over EGM96, whereas the retracked gravity field data by Laxon and McAdoo performs substantially better.

Table 2 Comparison with 1288 marine observations within the square bounded by 77°N to 79°N, and 5°W to 15°W from the Nordic gravity data base. All values are in mGal.

	Mean	Std Dev	Max dev.
EGM96	-0.76	17.63	122.91
Laxon&McAdoo (97)	1.10	6.59	56.21
KMS02	0.98	18.58	139.28
EAPRS 2 Hz	-2.10	5.78	43.93

6 Outlook

Within the coastal zone a variety of echo shapes can be returned to the altimeter. Some are caused by calmer patches of water, especially prevalent in sheltered areas and within coves and inlets. Others have been contaminated by the land, or show off-ranging to still inland water, especially close to river deltas or harbours.

However, even these complex shapes can be successfully retracked using the EAPRS expert system, vastly improving the data retrieval in coastal zones.

By using a new method to regress the 20 Hz ERS-1 geodetic mission altimetric data onto 2 Hz values corresponding to roughly 3.5km along track, we can obtain a spatial distribution of the altimetric data that has roughly the same along-track and across track spacing. On average it is 4 km across track spacing and 3.5 km along-track spacing.

Initial comparison with marine gravity field data already reveals that even at this preliminary stage (where residual offsets are known to exist between the different retrackers in the EAPRS system) we can obtain better comparison with the marine gravity observations than that obtained when using the data retracked by ESA.

Acknowledgment. The authors would like to thank R. Scharroo and colleagues for the 1 Hz (RADS) and ESA for providing waveform data for the analysis.

Information. The KMS2002 gravity field and the described gravity field (upon completion) will be available from the authors on CD-ROM (oa@spacecenter.dk) or from anonymous ftp at: ftp://ftp.kms.dk/pub/GRAVITY, www.research.dk/GRAVITY.

References

Andersen, O. B., and P. Knudsen, Global Marine Gravity Field from the ERS-1 and GEOSAT Geodetic Mission Altimetry, J. Geophys. Res., 103, 8129-8137, 1998.

Andersen, O. B., and Knudsen, P. The Role of Satellite Altimetry in Gravity Field Modelling in Coastal Areas, *Physics and Chemistry of the Earth (A),* Vol. 25, No. 1, pp. 17-24., 2000

Andersen, O. B., P. Knudsen, S. Kenyon and R. Trimmer, Recent improvement in the KMS global marine gravity field, Boll Geofis. teor. ed Applic. Vol, 40, 3-4, pp 369-377, 1999.

Andersen O. B. and P. Knudsen, Global Marine Gravity Field from the ERS-1 and GEOSAT Geodetic Mission Altimetry, *J. Geophys. Res., 103*(C4), 8129-8137, 1998.

Andersen, O. B., P. Knudsen and R. Trimmer, Improved high resolution gravity field mapping (the KMS02 Global Marine gravity field). In press, IAG symposium, 126, Sapporo, 2004

Berry, P.A.M., H. Bracke, and A. Jasper, 1997. Retracking ERS-1 altimeter waveforms over land for topographic height determination: an expert systems approach, ESA Pub. SP414 Vol. 1, 403-408.

Berry, P.A.M., J.D. Garlick, and E.L. Mathers, 2004. Global scale monitoring of land surface water using multi-mission satellite radar altimetry. EGU 1st General Assembly, Nice.

Challenor, P.G., and M.A. Srokosz, 1989. The extraction of geophysical parameters from radar altimeter return from a nonlinear ocean surface, in Brooks, S.R. (ed.) Mathematics in Remote Sensing, Institute of Mathematics and its Applications, pp 257-268.

Cleveland, W.S. (1979) "Robust Locally Weighted Regression and Smoothing Scatterplots," Journal of the American Statistical Association, Vol. 74, pp. 829-836.

Cleveland, W.S. and Devlin, S.J. (1988) "Locally Weighted Regression: An Approach to Regression Analysis by Local Fitting," Journal of the American Statistical Association, Vol. 83, pp. 596-610.

Fairhead , J. D., C. M. Green, K. M. U. Fletcher, Global mapping deep water hydrocarbon plays of the continental margins, ASEG 17th Geophysical conference and exhibition, Sydney, extended abstract, 2004,

Hwang, G. et. al., Satellite radar waveform retracking for improved coastal marine gravity anomaly accuracy in the Taiwan Strait., proceedings of the International Workshop on Satellite Altimetry for Geodesy, Geophysics and Oceanography: Summer Lecture Series and IAG symporium 126, 2003.

Laxon and McAdoo, 1998, Satellites Provide New Insights into Polar Geophysics, EOS, Transactions AGU, 79 (6), 69-72.

Sandwell, D. T., and Smith, W.H.F. Marine Gravity Anomaly from Geosat and ERS-1 Satellite Altimetry, Journal of Geophysical Research, Vol. 102, pp. 10039-10054, 1997.

Wang, Y. M. GSFC00 mean sea surface, gravity anomaly, and vertical gravity gradient from satellite altimeter data., J. Geophys res., 106, C12, 31167-31174, 2001

Space-borne gravimetry: determination of the time variable gravity field

P.N.A.M. Visser and E.J.O. Schrama
Department of Earth Observation and Space Systems (DEOS), Faculty of Aerospace Engineering, Delft University of Technology, Kluyverweg 1, 2629 HS, Delft, The Netherlands, Fax: +31 15 2785322, email: Pieter.Visser@lr.tudelft.nl, E.J.O.Schrama@lr.tudelft.nl

Abstract. The gravity field of the Earth can be divided into a dominant quasi-static part and several relatively small but significant temporal constituents. Important examples of temporal sources are ocean tides, atmospheric pressure variations, and geophysical signals like those of continental hydrology and ocean bottom pressure variations predicted by the ECCO ocean model. Space-borne gravimetry, such as by the GRACE system, aims at observing temporal changes of the Earth's gravity field, including those induced by continental hydrology. A case study, based on a simulated gravity field retrieval for a 1-year GRACE-type mission, has been conducted to analyze the separability of continental hydrology from other temporal gravity sources.

It has been investigated how typical differences between recent ocean tide models and between global atmospheric pressure variation maps affect the observations (low-low satellite-to-satellite range-rate tracking (SST) and orbital positions from GPS high-low SST) and retrieved gravity field spherical harmonic expansions. In addition, the aliasing of signals predicted by the ECCO model and the effect of low-low SST observation noise and uncertainties in the recovered orbital positions has been analyzed.

It is concluded that large scale features of continental hydrology can be observed by a GRACE-type mission, provided that the low-low SST observations have a precision at the level of 1 μm/s at 1 Hz, and when great care is taken with the gravity field recovery approach.

Key words. low-low satellite-to-satellite tracking, temporal gravity, hydrology, atmosphere, tides, ocean models

1 Introduction

Satellite Laser ranging (SLR) to satellites such as LAGEOS-1 and -2 has proved the possibility for observing temporal gravity in the very long wavelength domain leading for example to intriguing results for the time evolution of the Earth's oblateness or predominantly the J_2 term (Cox and Chao 2002; Cazenave and Nerem 2002). The CHAMP (launch July 15, 2000, (Reigber et al. 1999)) and GRACE (launch March 17, 2002, (Tapley and Reigber 1999)) satellite missions have opened the possibility for observing temporal gravity from space on a much more detailed scale than ever before and impressive results have already been obtained (Tapley et al. 2004). These results indicated the possibility for observing changes in continental hydrology in very large basins, such as in the Amazone area in South-America. However, results also indicated that great care needs to be taken when modeling other temporal gravity field sources such as ocean tides and changes in the atmospheric mass distribution. In addition, it was found that the gravity field reduction process is very sensitive to the parameterization of the gravity field estimation problem (arc length, empirical accelerations, accelerometer biases and scale factors). It was concluded that SLR tracking remains to be an important asset when analyzing geocenter variations (spherical harmonic degree 1 terms) and changes in J_2, and is a prerequisite for diagnosing possible problems in the processing of CHAMP and GRACE observations taken by the on-board science instruments.

The problem of temporal aliasing of different gravity field sources has been studied extensively,*cf.* (Han et al. 2004) and (Velicogna et al. 2001). We have built a simulation tool around the GEODYN software package (Rowlands et al. 1995) that allows to study the observability and separability of different gravity field sources (static and temporal) for several gravity field mission concepts and scenarios, including CHAMP- and GRACE-type missions, and possible future missions such as GOCE (ESA 1999) and GRACE/GOCE follow-ons. This tool allows a rigorous parameterization of the gravity field estimation problem and long data periods. It has been used for a case study where a one-year GRACE-type mission is defined for observing mass changes due to continental hydrology. The observability is studied in the presence of typical low-low SST observation noise levels and coupling with (errors in the modeling of) other temporal gravity field sources, including atmospheric mass redistributions, ocean tides and mass changes inflicted by ocean bottom pres-

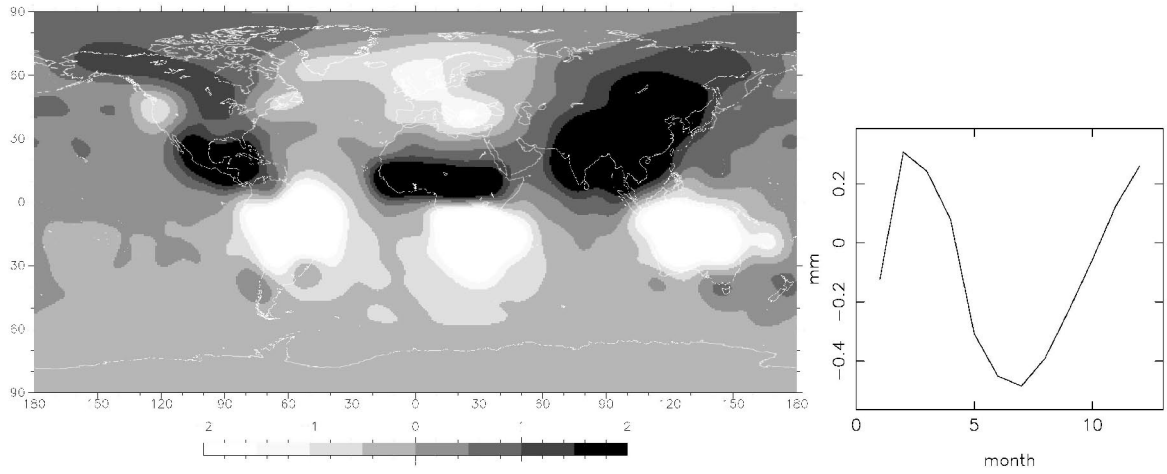

Fig. 1. Dominant mode (EOF) of mass changes due to continental hydrology for 2000 (Fan and van den Dool 2004). Please note the scale of the time pattern is in mm.

sure variations making use of ECCO ocean models (ECCO homepage 2004).

The simulation tool makes use of numerical integration of the equations of motion and variational equations for the estimated gravity field and orbit parameters, and offers the possibility to describe the Earth's gravity field as a sum of a baseline static part and (different) combinations of temporal sources. Currently all sources are represented by spherical harmonic expansions, although also space localized functions such as gravity anomalies and density layers are possible. For the case study to be outlined in the next section, the following models were used:

- Static gravity field model: GGM01S;
- Temporal gravity:
  - Continental hydrology (Fan and van den Dool 2004);
  - Ocean tides: FES99 and GOT99.2b;
  - Atmospheric mass variations: ECMWF and NCEP;
  - Ocean bottom pressure: ECCO.

The real world was modeled by the GGM01S static field (GRACE CSR home page 2004) in combination with GOT99.2b (Ray 1999) ocean tides, ECMWF based atmospheric mass variations, oceanic mass redistribution according to ECCO models, and continental hydrology (Fan and van den Dool 2004). The GGM01S model is a GRACE-based satellite only solution to degree and order 120, but was truncated at degree and order 50 in the case study. The two ocean tide models were derived using different methodologies. GOT99.2b is an empirical model, whereas FES99 makes use of hydrodynamical equations. The temporal background gravity field models were developed complete to degree and order 20 (making in certain cases for example use of Love numbers for converting equivalent water heights to Stokes coefficients, see (Schrama 2003)). Figure 1 displays the dominant mode (first EOF or Empirical Orthogonal Function) of the continental hydrology model in terms of geoid variations for a one year period. This dominant mode represents about 80% of the amplitude, or about 60% of the energy of the total signal. Clearly visible are relatively large fluctuations in the area covering part of the Southern states of the U.S, Mexico and Latin America, the area from the Sahel to South-Africa, the Amazone and Zambesi basins and areas in East-Asia. Also clearly visible is the dominant annual signature (right part of the Figure). The objective of the case study is to investigate whether this signature can be recovered by a GRACE-type mission in the presence of observation errors (low-low SST and GPS-based orbit reconstruction errors), mismodeling of ocean tides (using FES99 as reference model, (Lefèvre et al. 2002)) and atmospheric mass variations (using NCEP reanalysis surface pressure data as reference), and ignoring ECCO predicted gravity changes (see also Table 1). The static gravity field model is assumed to be a long-period averaged solution with negligible errors.

2 Temporal gravity

The signal and/or model uncertainty size derived from the spherical harmonic expansions of the different gravity field sources is displayed in Figure 2. In fact, for the atmospheric mass variations the signal size is the average of 366 daily spherical harmonic expansions complete to degree and order 20 (in the following referred to as 20x20) using daily pressure fields from the year 1992, for ECCO from 2000, and for continental hydrology the average of 12 monthly 20x20 fields for 2000. It can be seen that the error

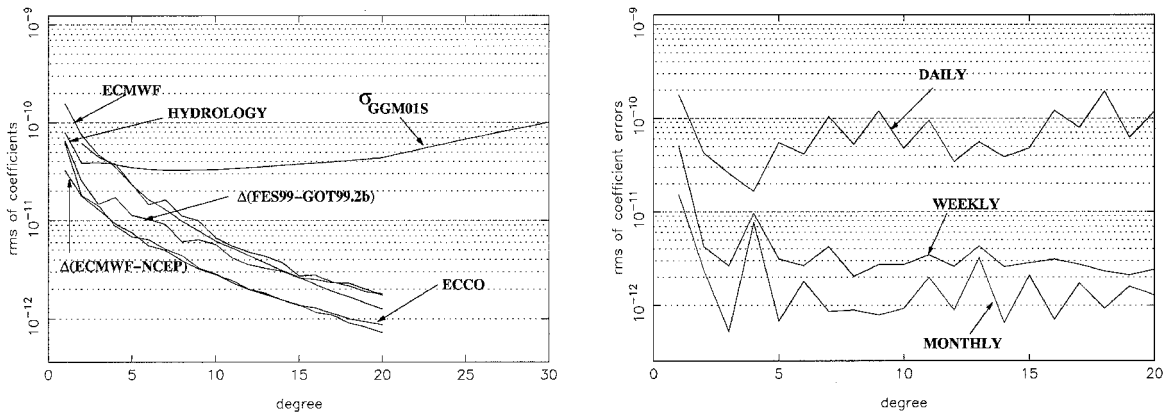

Fig. 2. Magnitude of temporal gravity field sources and model differences, and quality of GGM01S (left), and effect of observation noise on gravity field recovery accuracy for different observation period durations (right). The temporal gravity field sources include ocean tide model differences between FES99 and GOT99.2b, gravity field changes due to atmospheric mass redistributions (total signal according to ECMWF, and differences between ECMWF and NCEP), and gravity field variations due to continental hydrology and ECCO ocean models.

level of GGM01S, which is based on 111 days of GRACE observations, is above the signal size of continental hydrology up to degree 5. However, it is fair to assume that significant improvements will be made as time progresses resulting in more observations and a better understanding of the behavior of the GRACE system. Moreover, the objective is to study temporal gravity, although it is realized that errors in the static gravity field model might affect the recovery of temporal gravity, which is an interesting topic for future research. The signal size of the atmospheric mass variations is of the same order of magnitude as those inflicted by continental hydrology. Assuming that the differences between ECMWF and NCEP atmospheric pressure fields are representative for the accuracy with which atmospheric mass variations can be modeled, Δ(ECMWF-NCEP), continental hydrology can still be observed. The signal predicted by the ECCO model has a size comparable to the differences between the two atmospheric pressure field models and is in fact much below the continental hydrology signal. The uncertainty in ocean tide modeling, reflected by Δ(FES99-GOT99.2b), intersects the continental hydrology signal around spherical harmonic degree 15 (see Figure 2). Based on these results, it may be concluded that an effort is required to further improve ocean tide modeling.

3 Case study

Gravity field recovery simulation experiments have been conducted for a one year period, or 366 days for 2004 (leap year). It has to be noted that some temporal gravity sources that were used in the simulations are for 1992 and 2000 (Section 1). It is fair to assume that these data sets realistically reflect the signal magnitudes and time signatures that can be expected. A GRACE-type mission is selected, consisting of two satellites flying en echelon in 440 km altitude orbits with an inclination of 89° and separation of 200 km. Gravity field models are estimated from low-low SST observations and orbit positions (inertial Cartesian x, y, z coordinates) resolved from the GPS high-low SST observations. The low-low SST observations are sampled at 30-s intervals and Gaussian noise is added with a standard deviation of 0.2 μm/s (equivalent to 1 μm/s at 1 Hz). The orbit coordinates of the two satellites are assumed to have an accuracy of 1 cm (Gaussian) and are sampled at 2-min intervals (Table 1).

Table 1. Definition of case study: truth, reference and error models.

Truth model	
static gravity field:	GGM01S
continental hydrology:	Fan & Dool, 2004
ocean tides:	GOT99.2b
ocean bottom pressure:	ECCO
atmospheric pressure:	ECMWF
Reference model	
static gravity field:	GGM01S
continental hydrology:	none
ocean tides:	FES99
ocean bottom pressure:	none
atmospheric pressure:	NCEP
Observation errors (Gaussian)	
low-low SST:	$\sigma = 0.2$ μm/s @ 30-s
orbit coordinates:	$\sigma(x, y, z) = 1$ cm @ 2-min

The one-year simulated observation data set is divided into daily periods and for each day normal

equations are computed for a 20x20 spherical harmonic gravity field model (including degree 1 terms) and for epoch state vectors for the two satellites ($2 \times 6 = 12$ unknowns per day, each state vector consisting of 3 position and 3 velocity coordinates). It is fair to assume that above degree 20, the temporal gravity field signals have a very low signal magnitude (Figure 2) and it is also assumed that a high-accuracy, higher resolution background model is available for the static gravity field (in this case the 50x50 truncated GGM01S model). However, for future more advanced and precise gravity field missions, the simulations can be extended to (much) higher degrees, requiring extensive (but feasible) computer resources. The daily normal equations can be combined to obtain gravity field solutions for different period lengths. For example, a weekly solution is obtained by combining 7 daily normal equations solving for 84 (7×12) epoch state vector unknowns and one 20x20 gravity field spherical harmonic expansion.

4 Results

Before conducting the gravity field recovery in the presence of all error sources according to Table 1, the effect of different temporal gravity field sources on the low-low SST range-rate observations was assessed. The signal Root-Mean-Square (RMS) of the low-low SST range-rate observations is typically around 20 cm/s, and is dominated by the J_2 term. For all 366 days, the RMS is computed by estimating only the 12 (2×6) epoch state vector parameters. Finally, the RMS of the 366 daily RMS values is displayed in Table 2. Continental hydrology causes an RMS signal of about 0.18 μm/s, compared to 0.14 μm/s for the FES99/GOT99.2b ocean tide model differences, 0.43 μm/s for atmospheric mass variations predicted by ECMWF pressure fields, 0.22 μm/s for the differences between ECMWF and NCEP, and 0.10 μm/s for mass variations induced by the ECCO model. These numbers indicate that atmospheric mass variations need to be accurately modeled, that ocean tide model uncertainties compete with the continental hydrology signal and that the ECCO model results in relatively small low-low SST range-rate perturbations.

In a second step, the separate effect of observation errors on the achievable gravity field recovery error was assessed by generating 366 daily, 52 weekly and 12 monthly solutions. The annual averages of the degree RMS values of spherical harmonic coefficient errors is displayed in Figure 2. It can be seen that for weekly and monthly solutions the errors are below the continental hydrology signal, but that this is not the case for daily solutions (which can be anticipated considering that the satellites complete 16 orbital revolutions per day, but that a 20x20 model is solved for; in all cases no regularization was applied). The dominant error mode (EOF analysis) of the daily gravity field solutions in term of geoid is displayed in Figure 3 displaying a pattern commensurate with the daily ground tracks of the satellite pair. A similar pattern was predicted by an EOF analysis of the dominant eigenvectors of the daily inverses of the normal equations.

Table 2. RMS of low-low SST observation residuals (30-s sampling) due to different temporal gravity field sources (366 daily arcs)

Source	RMS (μm/s)
Continental hydrology:	0.179
Tide model differences:	0.142
Atmosphere: ECMWF	0.432
Atmosphere: ECMWF-NCEP	0.227
ECCO	0.101

Based on the previous results, it was decided to generate a time series of 52 weekly (or 52 7-day) gravity field solutions in the presence of all error sources listed in Table 1. Again, an EOF analysis was conducted. Figure 4 clearly reveals the dominant mode caused by errors in the recovery of degree 1 terms, which are heavily correlated with the 2×6 epoch state vector. It is obvious that the continental hydrology signal (Figure 1) is completely obscured by this mode. This error mode can again be predicted by error propagation, and thus seems to indicate an inherent weakness in the gravity field recovery approach (which might be solved by adding certain types of tracking data to other satellites, such as SLR tracking of LAGEOS-1/2). It was also found that the FES99 and GOT99.2b ocean tide model differences cause relatively large perturbations in the degree one gravity field terms indicating the need for co-estimation of tide model terms and/or independent tide model improvement. However, generating a second series of weekly gravity field solutions without solving for the degree one terms results in a dominant mode as displayed in Figure 5, clearly revealing the most important features of the continental hydrology signal (Figure 1). Striking differences can be observed in the Antarctic region, which can be attributed to large differences between the ECMWF and NCEP atmospheric pressure fields. Although the time signature is rather noisy, it displays a clear annual period comparable to the true annual pattern. It was found that this noisy behavior is reduced significantly when making monthly gravity field solutions.

It is interesting to compare as well the fourth EOF of the case where the gravity degree 1 terms (3 coefficients leading to possibly 3 dominant EOFs) are

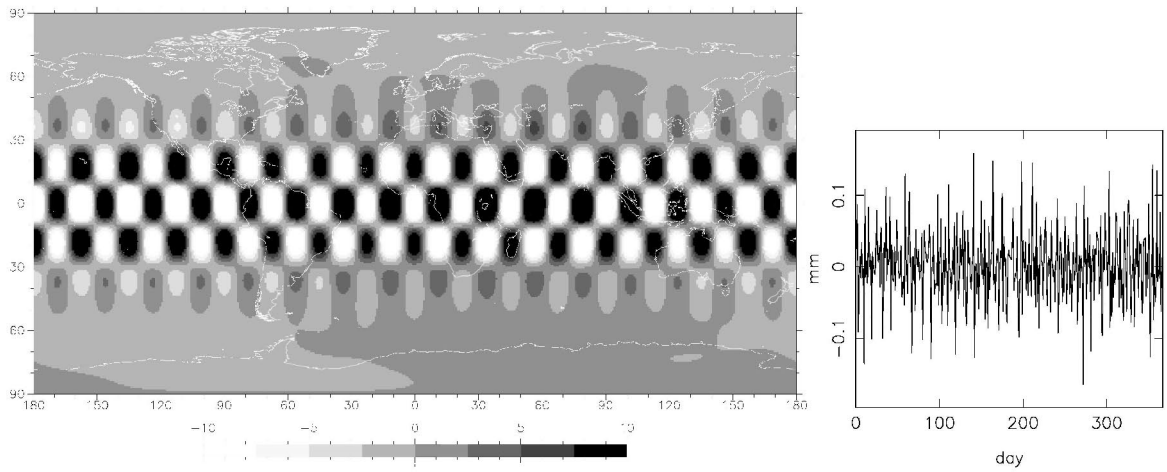

Fig. 3. Dominant mode (EOF) of recovered daily gravity field solutions with only observation noise switched on.

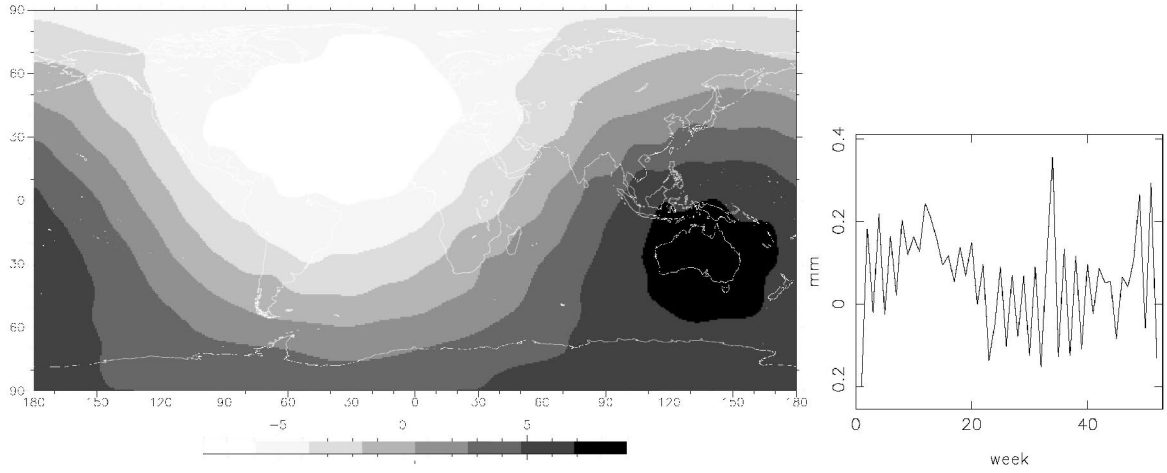

Fig. 4. Dominant mode (EOF) of recovered weekly gravity field solutions with all error sources switched on (degree one terms included).

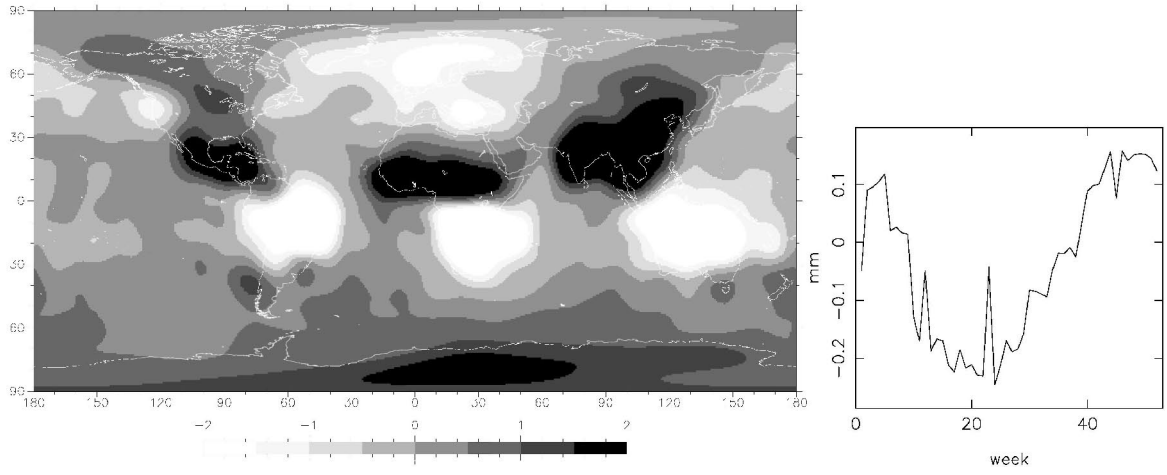

Fig. 5. Dominant mode (EOF) of recovered weekly gravity field solutions with all error sources switched on (degree one terms ignored).

estimated with the first EOF as displayed in Figure 4. It was found that these EOFs compare very well: the correlation is bigger than 90%.

5 Conclusions

Temporal gravity field variations such as induced by continental hydrology is observable with GRACE-type missions.

Great care needs to be taken with the parameterization of the gravity field recovery. First of all, the arc length and the combined estimation of non-gravitational (for example satellite epoch state vectors) and gravitational parameters needs to be carefully defined and investigated. Second, the period for which gravity field solutions are to be generated needs to be balanced with the required precision, temporal and spatial resolution levels.

It was found that the degree one terms can be seriously affected by uncertainties in ocean tide models. Also, there are indications that degree one terms are weakly observable by the investigated mission concept in combination with the adopted gravity field recovery approach. For overcoming this weakness, continued high-quality SLR tracking is instrumental and will in combination with GRACE-type observations guarantee high-precision temporal gravity modeling from the very long to the medium wavelength domain (degree 1 - 20).

The low-low SST observations need to have a high precision level, of the order of 1 μm/s at 1 Hz. In order to be able to observe continental hydrology, mass variations due to ocean tides and atmosphere need to be modeled with great precision.

Finally, it can be concluded that a tool has been implemented that can be used for gravity field mission analysis, opening the possibility to assess in a closed-loop the effect of observation noise, satellite configuration, mismodeling of (combinations of) gravity field sources and gravity field recovery reduction approach and parameterization.

Acknowledgments. The Center for Space Research, University of Texas at Austin, Texas, is acknowledged for providing the GGM01S model. The GEODYN software was kindly provided by the Goddard Space Flight Center, Greenbelt, Maryland. The ECCO models are a a contribution of the Consortium for Estimating the Circulation and Climate of the Ocean (ECCO) funded by the National Oceanographic Partnership Program. The ECCO models were converted to spherical harmonic expansions of equivalent water height and provided by J. Kusche, DEOS, Delft, The Netherlands.

References

Cazenave, A., and R.S. Nerem (2002), Redistributing Earth's Mass, *Science*, *297*, 783–784, August 2002.

Cox, C.M., and B.F. Chao (2002), Detection of Large-Scale Mass Redistribution in the Terrestrial System Since 1998, *Science*, *297*, 831–833, August 2002.

ECCO homepage, *http://www.ecco-group.org/*, last accessed: July 2004

ESA (1999), Gravity Field and Steady-State Ocean Circulation Mission, *Reports for Mission Selection, The Four Candidate Earth Explorer Core Missions, SP-1233(1)*, European Space Agency, July 1999.

Fan, Y., and H. van den Dool (2004), Climate Prediction Center global monthly soil moisture data set at 0.5° resolution for 1948 to present, *J. Geophys. Res.*, *109*(D10), 8 pp., May 2004.

GRACE CSR homepage, *http://www.csr.utexas.edu/grace/gravity*, last accessed: July 2004

Han, S.-C., C. Jekeli, and C.K. Shum (2004), Time-variable aliasing effects of ocean tides, atmosphere, and continental water mass on monthly mean GRACE gravity field, *J. Geophys. Res.*, *109*(B4), doi:10.1029/2003JB002501.

Lefèvre, F., F.H. Lyard, C. LeProvost, and E.J.O. Schrama (2002), FES99: A Global Tide Finite Element Solution Assimilating Tide Gauge and Altimetric Information, *Journal of Atmospheric and Oceanic Technology*, *19*(9), 1345–1356.

Ray, R D (1999), A global ocean tide model from Topex/Poseidon altimetry: GOT99.2, *NASA Tech. Memo. 209478*, 58 pp., Goddard Space Flight Center.

Reigber, Ch., P. Schwintzer, and H. Lühr (1999), The CHAMP geopotential mission, in *Bollettino di Geofisica Teorica ed Applicata, Vol. 40, No. 3-4, Sep.-Dec. 1999, Proceedings of the 2nd Joint Meeting of the International Gravity and the International Geoid Commission, Trieste 7-12 Sept. 1998, ISSN 0006-6729*, edited by I. Marson and H. Sünkel, pp. 285–289.

hspace*-3mm Rowlands, D., J.A. Marshall, J. McCarthy, D. Moore, D. Pavlis, S. Rowton, S. Luthcke, and L. Tsaoussi (1995), GEODYN II system description, Vols. 1-5, *Contractor report*, Hughes STX Corp., Greenbelt, MD.

Schrama, E.J.O. (2003), Error characteristics estimated from CHAMP, GRACE and GOCE derived geoids and from satellite altimetry derived mean dynamic topography, *Space Science Reviews*, *108*, 179–193.

Tapley, B.D., and C. Reigber (1999), GRACE: a satellite-to-satellite tracking geopotential mapping mission, in *Bollettino di Geofisica Teorica ed Applicata, Vol. 40, No. 3-4, Sep.-Dec. 1999, Proceedings of the 2nd Joint Meeting of the International Gravity and the International Geoid Commission, Trieste 7-12 Sept. 1998, ISSN 0006-6729*, edited by I. Marson and H. Sünkel, p. 291.

Tapley, B.D., S. Bettadpur, J.C. Ries, P.F. Thompson, and M.M. Watkins (2004), GRACE Measurements of Mass Variability in the Earth System, *Science*, *305*, 1503–505.

Velicogna, I., J. Wahr, and H. Van den Dool (2001), Can surface pressure be used to remove atmospheric contributions from GRACE data with sufficient accuracy to recover hydrological signals?, *J. Geophys. Res.*, *106*(B8), doi: 10.1029/2001JB900228.

Satellite clusters for future gravity field missions

Nico Sneeuw
Department of Geomatics Engineering, University of Calgary, sneeuw@ucalgary.ca,
currently at: Universität Stuttgart, Geodätisches Institut

Hanspeter Schaub
Aerospace and Ocean Engineering Department, Virginia Tech, schaub@vt.edu

Abstract. The current missions CHAMP and GRACE have already contributed drastically to our knowledge of the Earth's gravity field in terms of accuracy, homogeneity and time- and space-resolution. The future mission GOCE will further add to that in terms of spatial resolution. Nevertheless, each of these missions has its own limitations. At the same time several geoscience disciplines push for ever higher requirements on spatial resolution, time resolution and accuracy. Future gravity field missions will need to address these requirements.

A number of new technologies may enable these future missions. They include laser tracking and atomic interference. Most likely, a mission that implements such technologies, will make use of the concept of formation flying. This paper will discuss the feasibility of low-Earth satellite clusters. It focuses in particular on the stability of satellite formations under the influence of perturbations by the Earth's flattening. Depending on initial conditions several types of relative J_2 orbits can be attained.

By interpreting the low-low satellite-to-satellite tracking observable as gradiometry this paper furthermore indicates how satellite clusters may be employed in satellite gravimetry.

1 Limitations of current and planned gravity missions

CHAMP, GRACE and GOCE. The satellite mission CHAMP currently provides static gravity field solutions at dm-level geoid accuracy up to an effective maximum spherical harmonic degree of around 60, cf figure 1. Recovery of the time-variable field seems to be at—or rather below—the edge of feasibility. Although CHAMP is still in orbit, delivering quality science data, this combination of resolution and accuracy is the natural limitation of the mission.

The accuracy of GRACE-derived geoids, on the other hand, is at mm-level around these degrees. It achieves its resolution around degree 120 at which the geoid accuracy is at the dm-level again. Future data and modeling improvements will likely push the limit towards a maximum degree of 150. Moreover, GRACE provides monthly solutions that clearly reveal time-variable gravity (Tapley et al., 2004).

The gradiometer mission GOCE, due for launch in 2006, aims at cm-accuracy and a spatial resolution corresponding to maximum degree 300. This high resolution, combined with the relatively short mission duration, does not allow time-variable gravity recovery, although time variations will alias into the static solution.

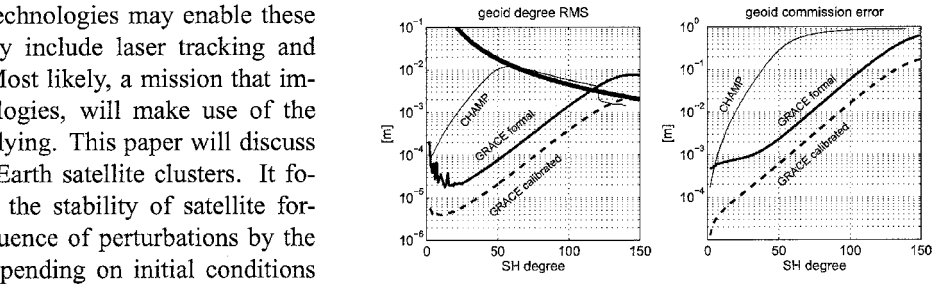

Fig. 1. CHAMP and GRACE gravity recovery performance: geoid RMS (left) and cumulative geoid error (right) as function of spherical harmonic degree. The CHAMP curves represent the model EIGEN2. Those of GRACE refer to EIGEN-GRACE02S.

Despite the wealth of new gravity field information and despite the many new scientific issues that can be addressed, these missions are limited in spatial resolution, temporal behaviour (resolution and mission duration) and accuracy of the resulting gravity field recovery. The key limitations, at least from a gravity recovery viewpoint, are:

- Sampling and resolution: missions are designed for either spatial or spectral resolution. A simultaneous high spatial and spectral resolution is fundamentally impossible with a single mission.
- Aliasing: unmodeled phenomena with submonthly period will alias into the monthly GRACE solutions. Time-variable signal will also map into the static GOCE field.
- Monitoring: limited mission durations of 5 year

(CHAMP, GRACE) or 1 year (GOCE).

- Gravity signal: when interpreted as an along-track gravity gradient, the GRACE-observable is seen to be a relatively weak component, see below.

The limitations of GRACE and GOCE are analyzed from a more technological viewpoint by Aguirre-Martinez and Sneeuw (2003).

Future low-low SST. At the same time Earth scientist are driving the requirements for ever higher accuracies and resolutions. Moreover, similar to satellite radar altimetry, there is a growing demand for a monitoring facility rather than a few individual satellite missions. Studies into next-generation gravity field missions tend to focus on low-low satellite-to-satellite tracking (SST). Indeed, the accuracy gain that is potentially achieved by laser SST over a GRACE-type radio link is far larger than the expected future improvements in gradiometry technologies.

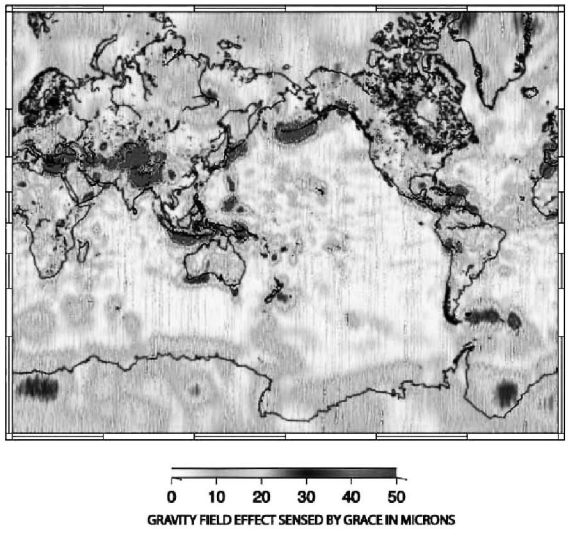

Fig. 2. GRACE *first light*: map of gravity field effect on inter-satellite baseline.

The key GRACE-type SST observable is the inter-satellite distance and relative velocity in a leader-follower configuration at near-polar inclination. This type of observable inherently suffers from the weakness that it is mainly sensitive along the line-of-sight, i.e. in North-South direction. This was demonstrated by the very first release of a GRACE map, cf. Figure 2, which clearly demonstrated a sensitivity towards East-West features in the Earth's gravity field. Note, for instance, the weak presence of Andes or Rocky Mountains in the map.

The observable approximates the along-track inline gravity gradient term V_{xx}. In terms of gravity gradiometry this is known to be a relatively weak term. Its spectral content is approximately one half of the radial gravity gradient term V_{zz}. More importantly, the directional sensitivity of the observable also translates into a non-isotropic error behaviour.

Formation flying. Formation flying, which is currently receiving much attention internationally, may solve some of the aforementioned issues. A satellite formation may consist of any number of satellites that are performing a relative motion around a common center. A GRACE-type leader-follower formation can be seen as a simple example of formation flight. In general, satellites may perform more complicated elliptical or circular relative motion. Obviously, when the distances between these satellites would be measured, the gravitational signal would include radial information. Moreover, a relative inclination might be achieved that would lead to cross-track information going into the observable. Such observables could address several of the aforementioned weaknesses, most notably the spectral content and the non-isotropy of the low-low SST observable. Including cross-track information may also reduce the aliasing problem.

For these reasons this paper will mainly investigate the feasibility of formation flying in a realistic gravity field. It will then be discussed how to use formation flying in a gravity field mission.

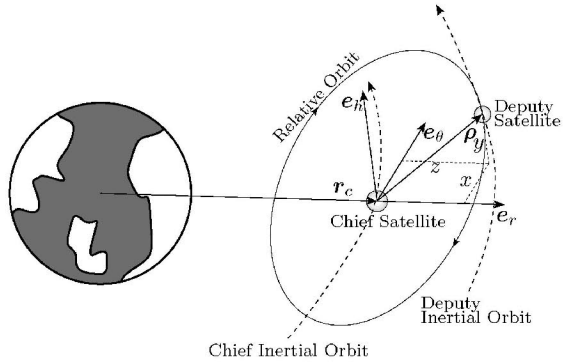

Fig. 3. Illustration of a general spacecraft formation with out-of-plane relative motion.

2 Feasibility of formation flying in a J_2 gravity field

2.1 Equations of relative motion

Let us adopt the following formation flying notation. A set of deputy satellites are to fly about a

chief location as shown in Figure 3. This location could be an actual spacecraft, or simply a reference point. The inertial chief position vector is $\boldsymbol{r}_c$, while $\boldsymbol{\rho}$ is the deputy relative position vector. The rotating Hill frame $\mathcal{O} = \{\boldsymbol{e}_\theta, \boldsymbol{e}_h, \boldsymbol{e}_r\}$ is defined with $\boldsymbol{e}_r$ being along the chief orbit radial, $\boldsymbol{e}_h$ being along the chief orbit plane normal, and $\boldsymbol{e}_\theta$ completing the right handed coordinate system. The angular rate of the Hill frame (chief motion) is $\dot{\theta}$. The deputy position vector $\boldsymbol{\rho}$ is then expressed in the Hill frame through

$$^{\mathcal{O}}\boldsymbol{\rho} = (x, y, z)^T \tag{1}$$

The general equations of motion of a deputy satellite with respect to a chief is given by Schaub and Junkins (2003):

$$\ddot{x} + z\ddot{\theta} + 2\dot{z}\dot{\theta} - x\left(\dot{\theta}^2 - \frac{\mu}{r_c^3}\right) = a_x \tag{2a}$$

$$\ddot{y} + \frac{\mu}{r_c^3} y = a_y \tag{2b}$$

$$\ddot{z} - z\left(\dot{\theta}^2 + 2\frac{\mu}{r_c^3}\right) - x\ddot{\theta} - 2\dot{x}\dot{\theta} = a_z \tag{2c}$$

where μ is the gravitational constant and (a_x, a_y, a_z) are non-Keplerian forces acting on the deputy satellite. They could be due to atmospheric drag, J_2 gravitational oblateness effects, or control thrusters.

Many missions consider formations where the chief motion is essentially circular with a near zero eccentricity e. In this case the chief rate $\dot{\theta}$ is constant and equal to the mean orbit rate $n = \sqrt{\mu/r_c^3}$. The equations of motion simplify to the well-known linearized Hill equations (Hill, 1878), see also (Clohessy and Wiltshire, 1960):

$$\ddot{x} + 2n\dot{z} = a_x \tag{3a}$$

$$\ddot{y} + n^2 y = a_y \tag{3b}$$

$$\ddot{z} - 2n\dot{x} - 3n^2 z = a_z \tag{3c}$$

We will refer to them as HE in the sequel. Eq. (3) has been used extensively in spacecraft formation flying mission analysis and control research. They are reasonable as long as (x, y, z) are small compared to the chief orbit radius r_c.

Often it is convenient to work in non-dimensional states. Let $(u, v, w) = (x, y, z)/r_c$ be non-dimensional deputy relative position coordinates. If the true anomaly f is used as the independent angle instead of time, then the general first order equations of motion are given through:

$$u'' + 2w' = \alpha_u \tag{4a}$$

$$v'' + v = \alpha_v \tag{4b}$$

$$w'' - 2vv' - \frac{3w}{1 + e\cos f} = \alpha_w \tag{4c}$$

Many further forms of the relative motion have been developed. Schweighart and Sedwick (2002) developed an extension to the HE which includes linear J_2 oblateness perturbations in the equations of motion. Humi and Carter (2003) have shown solutions with special forms of quadratic drag. An excellent survey of relative motion state transition matrices is found in (Carter, 1998).

2.2 First order analytical solutions

If the chief motion can be modeled as circular, then the HE can be solved analytically. Assuming no perturbations or thrusting is present ($a_x = a_y = a_z = 0$), all possible deputy relative motions can be expressed in closed form (Schaub and Junkins, 2003):

$$x(t) = -2A_0 \sin(nt + \alpha) - \frac{3}{2} n t z_{\text{off}} + x_{\text{off}} \tag{5a}$$

$$y(t) = B_0 \cos(nt + \beta) \tag{5b}$$

$$z(t) = A_0 \cos(nt + \alpha) + z_{\text{off}} \tag{5c}$$

Note that the out-of-plane motion is decoupled from the in-plane motion. The integration constants can be expressed in terms of initial conditions through:

$$A_0 = \frac{1}{n}\sqrt{\dot{z}_0^2 + (2\dot{x}_0 + 3nz_0)^2} \tag{6a}$$

$$B_0 = \frac{1}{n}\sqrt{\dot{y}_0^2 + (ny_0)^2} \tag{6b}$$

$$\alpha = \arctan\left(\frac{\dot{z}_0}{3nz_0 + 2\dot{x}_0}\right) \tag{6c}$$

$$\beta = \arctan\left(\frac{-\dot{y}_0}{ny_0}\right) \tag{6d}$$

$$z_{\text{off}} = \frac{2}{n}(\dot{x}_0 + 2nz_0) \tag{6e}$$

$$x_{\text{off}} = x_0 - \frac{2\dot{z}_0}{n} \tag{6f}$$

These equations are very convenient to explore what possible *natural* and unforced formation shapes are feasible. For example:

- If $B_0 = 0$, a purely in-plane relative motion is achieved which is always a 2:1 ellipse (the CartWheel-mode);
- If $B_0 = \sqrt{3}A_0$, the relative motion is circular with radius $2A_0$ (the LISA-mode);

– If $B_0 = 2A_0$, one achieves elliptical motion with a circular cross-section in the local horizon plane $\boldsymbol{e}_\theta$-$\boldsymbol{e}_h$ (the TechSat21-mode).

The latter two configurations also require either $\alpha = \beta$ or $\alpha = \beta + \pi$.

If the chief motion is not circular, then the solution in Eq. (5) is no longer valid. Even small amounts of eccentricity can produce modeling errors comparable to those produced by J_2 gravitational perturbations or atmospheric drag. Carter (1998) presents an analytical solution to the linearized relative motion where the true anomaly is used as the independent variable. However, this solution does not provide that elegant geometrical insight the classical HE solution provides. In (Schaub, 2004) the first order (u, v, w) non-dimensional relative motion is expressed in terms of orbit element differences. This analytical relative motion solution is valid for chief motions of any eccentricity, but also uses true anomaly as the independent variable. The orbit element difference based solution is written in terms of static offsets and sinusoidal components, and has a similar geometric structure as the analytical HE solution. Even for highly eccentric chief motions, the first order out-of-plane relative motion is still decoupled from the in-plane motion.

2.3 Bounded relative motion constraints

To avoid having the formation drift apart, bounded relative motion solutions are sought. If no perturbations are present, then the nonlinear bounded relative motion constraint is simply that all orbit periods must be equal. This is equivalent to requiring that the semi-major axis differences δa be zero. This bounded motion constraint is valid for both circular and eccentric orbits, as well as small and large relative orbit dimensions.

The orbit element constraint $\delta a = 0$ can be approximated using Hill frame Cartesian coordinates by taking a first order expansion. An equivalent approach is to look at the analytical HE solution in Eq. (5). The only secular growth occurs in the along track direction through the $-3/2nt z_{\text{off}}$ term. For this secular growth term to be zero, we find that the initial Cartesian coordinate conditions must satisfy

$$\dot{x}_0 + 2nz_0 = 0 \tag{7}$$

This first order approximation of $\delta a = 0$ assumes that the chief is circular and that the relative orbit radius ρ is small compared to the chief orbit radius r_c. However, this condition can be applied at any point within the orbit. If the chief motion has a small but non-zero eccentricity, then the first order bounded relative motion constraint is written as (Inalhan et al., 2002; Schaub and Junkins, 2003):

$$\dot{x}_0 + (2 + 3e)nz_0 = 0 \tag{8}$$

if the initial time is set at perigee.

If the gravitational J_2 perturbation is present, then all orbits experience short and long period perturbations. Only the ascending node Ω, argument of periapsis ω and initial mean anomaly M_0 will experience secular drift. Their mean rates are given by (Schaub, 2004; Schaub and Alfriend, 2001):

$$\frac{\mathrm{d}\Omega}{\mathrm{d}t} = -\frac{\epsilon(a,e)}{2} n \cos i \tag{9a}$$

$$\frac{\mathrm{d}\omega}{\mathrm{d}t} = \frac{\epsilon(a,e)}{4} n \left(5\cos^2 i - 1\right) \tag{9b}$$

$$\frac{\mathrm{d}M_0}{\mathrm{d}t} = \frac{\epsilon(a,e)}{4} n\eta \left(3\cos^2 i - 1\right) \tag{9c}$$

with $\epsilon(a,e) = 3J_2\left(r_{\text{eq}}/a(1-e^2)\right)^2$ and where $\eta = \sqrt{1-e^2}$ is an eccentricity measure. The distance r_{eq} is Earth's equatorial radius. Note that only a, e and i control the secular drift rate of the remaining three orbit elements. This drift could be compensated for by thrusting. However, this will quickly consume a lot of fuel. Schaub and Alfriend (2001) introduce the concept of J_2-invariant relative orbits. Here the relative orbit geometry is designed such that while all orbits are still drifting, on average, they will drift at equal rates. To achieve this, the following mean relative drift rates are set to zero:

$$\delta\dot{\theta} = \delta\dot{\omega} + \delta\dot{M}_0 = 0 \tag{10a}$$

$$\delta\dot{\Omega} = 0 \tag{10b}$$

The first condition guarantees no in-plane drift and leads to the orbit element constraint equation

$$\frac{\delta a}{a} = \frac{J_2}{2}\frac{a^2}{r_{\text{eq}}^2}\frac{1}{\eta}(4+3\eta)(1+5\cos^2 i)\delta\eta \tag{11a}$$

The second conditions controls the out-of-plane drift. It yields the orbit element constraint

$$\delta\eta = -\frac{\eta}{4}\tan i\,\delta i \tag{11b}$$

By choosing either a difference in eccentricity, inclination, or semi-major axis, the other two orbit element differences are then dictated through the constraints in Eqs. (11a) and (11b). Note that in order to have either a difference in eccentricity or inclination, a non-zero difference in semi-major axis is required.

This is a departure from the Keplerian bounded relative motion results. For near-polar chief motions with inclination differences, the J_2-invariance constraints may result in very large along-track relative orbit dimensions. To avoid this, the 2nd constraint (11b) is typically dropped and any out-of-plane secular drift will have to be compensated for through thrusting (Schaub and Junkins, 2003). When designing J_2-invariant relative orbits, the motion is typically described in mean element space, cf. (Schaub and Alfriend, 2001; Brouwer, 1959). To map between the osculating (instantaneous) orbit elements and the mean orbit elements (long period and secular terms removed), the Brouwer-Lyddane theory can be used (Lyddane, 1963; Brouwer, 1959).

3 Gravity mapping from satellite formations

Future low-low sst missions, whether formation flying or not, will most likely employ laser technology for the intersatellite link. Bender et al. (2003) discuss heterodyne laser interferometry, whereas McGuirk et al. (2002) discuss atomic interference. Differential accelerometry seems feasible at a level of $10^{-12}\,\mathrm{m\,s^{-2}}/\sqrt{\mathrm{Hz}}$. Over a baseline of 1 km this would translate already into gradiometry at the $10^{-6}\,\mathrm{E}/\sqrt{\mathrm{Hz}}$ level. The baseline length immediately scales into the error level.

The range rate $\dot{\rho}$ between two satellites is the projection of the relative vectorial velocity $\dot{\boldsymbol{\rho}}$ on the line-of-sight unit vector $\boldsymbol{e}$, e.g. (Rummel et al., 1978):

$$\dot{\rho} = \dot{\boldsymbol{\rho}} \cdot \boldsymbol{e} \tag{12a}$$

$$\Rightarrow \ddot{\rho} = \ddot{\boldsymbol{\rho}} \cdot \boldsymbol{e} + \frac{1}{\rho}\left(\dot{\boldsymbol{\rho}} \cdot \dot{\boldsymbol{\rho}} - \dot{\rho}^2\right) \tag{12b}$$

Using Newton's equations, the vectorial acceleration difference $\ddot{\boldsymbol{\rho}}$ equals the difference in gravitational attraction ∇V between the forces. The scalar range acceleration $\ddot{\rho}$ can be obtained from the observed range rate by numerical differentiation. To extract the gravitational information, one should further correct for the relative velocity terms at the right of (12b).

Gradiometry from satellite formations. Alternatively, when dividing $\ddot{\boldsymbol{\rho}} \cdot \boldsymbol{e}$ by the baseline, one obtains the in-line gravity gradient in the baseline direction $\boldsymbol{e}^{\mathrm{T}}\boldsymbol{V}\boldsymbol{e}$, with $\boldsymbol{V}$ the gravity gradient tensor. With the baseline close to along-track direction, this observable is mainly V_{xx}. Again, one should correct for the relative velocity terms at the right hand side of (12b). Moreover, one has to account for a linearization error in the approximation $V_{xx} \approx (V_{x,2} - V_{x,1})/(x_2 - x_1)$.

In a satellite formation, the baseline performs a full revolution in the Hill frame $\mathcal{O}$, i.e. the direction $\boldsymbol{e}$ rotates once every orbital revolution. Thus the observed gravity gradient $\boldsymbol{e}^{\mathrm{T}}\boldsymbol{V}\boldsymbol{e}$ contains projections of several tensor components V_{ij}, $i,j \in \{x,y,z\}$. The gravity gradient tensor $\boldsymbol{V}$ transforms under a rotation of the coordinate frame as $R\boldsymbol{V}R^{\mathrm{T}}$, in which R denotes the rotation matrix. Let us consider one satellite pair only in the simplest formation, namely the 2:1-ellipse in the orbital plane. Now assume a time-variable rotation α about the y-axis, such that the two satellites are always on the new x'-axis. The coplanar gradients V_{xx}, V_{xz}, V_{zz} project onto the observable as follows:

$$V_{x'x'} = \cos^2\alpha V_{xx} + 2\cos\alpha\sin\alpha V_{xz} + \sin^2\alpha V_{zz}$$

The observable $V_{x'x'}$ $(= \boldsymbol{e}^{\mathrm{T}}\boldsymbol{V}\boldsymbol{e})$ contains the required gravity observable already. However, if one wants to disentangle the 3 contributing tensor components in the Hill frame, 3 independent intersatellite distances need to be tracked. With 3 different angles α one would have 3 simultaneous equations of the above kind, leading to an instantaneous determination of V_{xx}, V_{xz} and V_{zz}. This can either be realized by a CartWheel of 3 satellites, measuring in a triangle, or by 6 satellites, measuring along the spokes of the wheel, cf. figure 4. The spokes configuration may be easier to realize at the cost of more satellites. The intersatellite links in the triangular formation are dependent. Technologically that may be more demanding, but it has the added benefit that the required orientations are better constrained.

Fig. 4. Potential coplanar configurations for measuring the in-plane V_{xx}, V_{xz} and V_{zz} simultaneously: triangle edges (left) or spokes (right).

Gradiometry of out-of-plane components (V_{xy}, V_{yy}, V_{yz}) can only be achieved through non-coplanar satellite configurations. A relative inclination of the formation w.r.t. the orbit plane can be represented by a rotation $R_x(\beta)$. Along the same lines of arguing as above it can be demonstrated that all gravity gradient tensor components will generally project onto a particular $V_{x'x'}$. To disentangle this projection, 6 instantaneous intersatellite distances should be measured. Thus formation flying offers a way of full-tensor gravity gradiometry.

4 Conclusion

When designing future gravity field missions, formation flying is a viable alternative to leader-follower low-low SST configurations. Despite the presence of perturbations—the strongest being the Earth's oblateness—stable configurations exist. The homogeneous Hill equations demonstrate which natural formation shapes are possible. In its simplest form, a 2:1 relative ellipse, the radial gravity gradient V_{zz} is projected onto the SST observable. Thus, the inherent weakness and the non-isotropic behaviour of the conventional low-low SST observable can be solved by formation flying.

Gravity field recovery can be based on observed range rates $\dot{\rho}$. Alternatively they may be differentiated numerically into $\ddot{\rho}$, which can be interpreted as differences in the gravitational attraction between the satellites. Moreover, $\ddot{\rho}$ can be recast into a gravity gradient observable $e^{\mathrm{T}}Ve$. With sufficiently many satellites linked together in a strategic way, one can even achieve full-tensor gravity gradiometry.

If the relative orbits comprise a cross-track motion, the corresponding observables gain sensitivity in East-West direction. Although this may be helpful in dealiasing signals, the fundamental temporal-spatial sampling problem of a gravity field satellite mission is not addressed. To overcome aliasing multiple-formation configurations must be considered, such as the planned geomagnetic field mission SWARM: one satellite pair at the same altitude but with different right-ascension, plus a single higher satellite.

These results are only the first step towards establishing formation flying technology as a powerful tool for future gravity field satellite missions. In future closed-loop simulations the gravity recovery performance of such missions must be carefully assessed under a variety of mission parameters and formation designs. Moreover, it is obvious that such missions will prompt further technological questions, e.g. into orbit-, attitude- and drag-control. These and other issues must be addressed in future studies.

Finally, if the individual satellites can be designed and launched in a cost-effective way, a formation flying mission would be suitable as a long-term monitoring mission.

Acknowledgments. Nico Sneeuw gratefully acknowledges the support of the Alexander von Humboldt Foundation and of the GEOIDE Network of Centres of Excellence.

References

Aguirre-Martinez, M. and Sneeuw, N. (2003). Needs and tools for future gravity measuring missions. *Space Science Reviews*, 108(1-2):409–416.

Bender, P. L., Hall, J. L., Ye, J., and Klipstein, W. M. (2003). Satellite-satellite laser links for future gravity missions. *Space Science Reviews*, 108(1-2):377–384.

Brouwer, D. (1959). Solution of the problem of artificial satellite theory without drag. *The Astronomical Journal*, 64(1274):378–397.

Carter, T. E. (1998). State transition matrix for terminal rendezvous studies: Brief survey and new example. *Journal of Guidance, Control and Dynamics*, 31(1):148–155.

Clohessy, W. H. and Wiltshire, R. S. (1960). Terminal guidance system for satellite rendezvous. *Journal of the Aerospace Sciences*, 27(9):653–658.

Hill, G. W. (1878). Researches in the lunar theory. *Am. Journal of Math.*, I:5–26,129–147,245–260.

Humi, M. and Carter, T. (2003). The Clohessy-Wiltshire equations can be modified to include quadratic drag. In *Proc. AAS/AIAA Space Flight Mechanics Meeting*, number AAS 03–240, Ponce, Puerto Rico. AAS/AIAA.

Inalhan, G., Tillerson, M., and How, J. P. (2002). Relative dynamics & control of spacecraft formations in eccentric orbits. *Journal of Guidance, Control and Dynamics*, 25(1):48–59.

Lyddane, R. H. (1963). Small eccentricities or inclinations in the Brouwer theory of the artificial satellite. *The Astronomical Journal*, 68(8):555–558.

McGuirk, J. M., Foster, G. T., Fixler, J. B., Snadden, M. J., and Kasevich, M. A. (2002). Sensitive absolute-gravity gradiometry using atom interferometry. *Physical Review A*, 65:doi 10.1103/PhysRevA.65.033608.

Rummel, R., Reigber, Ch., and Ilk, K.-H. (1978). The use of satellite-to-satellite tracking for gravity parameter recovery. In *Proc. European Workshop On Space Oceanography, Navigation And Geodynamics (SONG)*, volume SP-137, pages 153–161, Schloss Elmau. ESA.

Schaub, H. (2004). Relative orbit geometry through classical orbit element differences. *Journal of Guidance, Control and Dynamics*, 27(5):839–848.

Schaub, H. and Alfriend, K. T. (2001). J_2 invariant relative orbits for spacecraft formations. *Celestial Mechanics and Dynamical Astronomy*, 79(2):77–95.

Schaub, H. and Junkins, J. L. (2003). *Analytical Mechanics of Space Systems*. AIAA Education Series, Reston, VA.

Schweighart, S. A. and Sedwick, R. J. (2002). A high fidelity linearized J_2 model for satellite formation flight. *Journal of Guidance, Control, and Dynamics*, 6(25):1073–1080.

Tapley, B. D., Bettadpur, S., Ries, J. C., Thompson, P. F., and Watkins, M. M. (2004). GRACE measurement of mass variability in the Earth system. *Science*, 305:503–505.